PROCEEDINGS, 42nd Workshop on Geothermal Reservoir Engineering
Stanford University, Stanford, California, February 13-15, 2017
SGP-TR-212

Occurrences of Clay Minerals in Permeable Fracture Zones in the Granitic Basement of Geothermal Wells at Rittershoffen, France

Jeanne Vidal[1*], Patricia Patrier[2], Albert Genter [3], Daniel Beaufort[2]

[1]University of Strasbourg, CNRS UMR 7516 IPGS, 1 rue Blessig, F-67084 Strasbourg Cedex

[2]University of Poitiers, CNRS UMR 7285 IC2MP, HydrASA, Bat B8, Rue Albert Turpain, F-86022 Poitiers Cedex

[3]ES-Géothermie, 5 rue de Lisbonne, F-67300 Schiltigheim

*j.vidal@unistra.fr

Keywords: permeable fracture zones, hydrothermal alteration, clay minerals, Enhanced Geothermal System, Rittershoffen, Upper Rhine Graben

ABSTRACT

Two geothermal wells, GRT-1 and GRT-2, were drilled in a granite at Rittershoffen (Alsace, France), in the Upper Rhine Graben, in order to exploit the geothermal resource at the sediment-basement reservoir. Brine circulations occur in a permeable fracture network and lead to hydrothermal alteration. The goal of the study is to characterize the hydrothermal alteration associated with permeable fracture zones in Rittershoffen. As clay minerals are very reactive to hydrothermal alteration and could be good indicator to past and present circulations. A special attention has been paid to the textural, structural and chemical properties of these minerals. The clay fractions (<5 μm) were analyzed in fifty cuttings samples selected around permeable fracture zones in order to analyze the microstructural properties of clays from X-Ray Diffraction and the chemical composition of clays from Scanning Electron Microscope coupled with EDS. Chloritization (ferromagnesian chlorites) and sericitization (well crystallized illite) associated with pervasive alteration are observed along wells. Iron-rich chloritic materials were observed in fracture fillings as well as illitic materials enriched in poorly crystallized illite and I/S mixed layers (<10% of smectite) related to hydrothermal alteration as evidenced in both wells in permeable fracture zones. The heterogeneous assemblages of I/S mixed layers and the small-size of illite crystallites could be a response to an abrupt change of physical and chemical conditions such as the mixing of an oversaturated ascending geothermal fluid with a cooler fluid favoring nucleation of metastable phases. The intense illitization associated with fluid circulations may lead to a total replacement of chloritic materials as observed in the major permeable fracture zone of GRT-1 and a reduction of the natural permeability. The well GRT-2 presents four permeable fracture zones in the granitic basement with a good natural permeability probably because they are less affected by illitization.

1. INTRODUCTION

The Upper Rhine Graben (URG) is a geological structure located between Germany, France and Switzerland (Figure 1). This Cenozoic rift hosts several geothermal anomalies associated with hydrothermal circulations through the fracture network at the sediments-basement interface (Pribnow and Schellschmidt, 2000; Schellschmidt and Clauser, 1996). Between 2012 and 2014, a geothermal doublet (GRT-1, GRT-2) was drilled at 2.6 km depth TVD in Rittershoffen (Alsace, France) in order to exploit the local geothermal anomaly. The boreholes targeted the local normal fault of Rittershoffen (Figure 1). Both wells intersected the natural permeable fracture network associated to the Rittershoffen fault at the sediment-basement interface. The geological characterization of this natural permeable fracture network at the borehole scale is an important milestone for industrial project because it channels the present geothermal fluids. At Rittershoffen, the natural fracture network intersected was structurally investigated from various geophysical logs including acoustic image logs in open-hole section of the wells GRT-1 and GRT-2 (Vidal et al., 2016a).

Structural analysis was correlated with permeability indication such as temperature anomalies and/or mud losses during drilling operations in order to identify permeable fracture zones (Figure 2). One permeable fracture zone was observed in the granitic basement of GRT-1 whereas no obvious evidence of permeability was observed in sandstones. Four permeable zones were observed in the granitic basement of GRT-2 (Baujard et al., 2017).

Special attention has been paid to the "clay signature" of these permeable fracture zones in the granitic basement. Due to their reactivity to the physico-chemical environment, clay minerals have been used as markers of paleoconditions in both fossil and active geothermal systems. Mineralogical studies of clay fraction have proved to be an efficient approach to mark the circulation zones in high-temperature systems (Beaufort et al., 1992; Flexser, 1991; Mas et al., 2006; Patrier et al., 1996; Reyes, 1990; Teklemariam et al., 1996) but are poorly applied to Hydrothermal Systems in the URG. In this study, clay fraction of cuttings from GRT-1 and GRT-2 was analyzed by X-Ray Diffraction (XRD) in order to analyze crystal structures of clay minerals and Scanning Electron Microscope (SEM) coupled with EDS in order to analyze chemical composition of clay minerals. As fracture permeability is a key challenge in this geothermal project, most of the samples were collected around permeable fracture zones of both wells.

2. GEOLOGICAL CONTEXT

The Rittershoffen site is located in the URG, less than 10 km from the well-known Soultz-sous-Forêts site (Alsace, France) and approximately 15 km east of the Western Rhenian fault, which strikes N45°E in this part of the graben (Figure 1). A geothermal doublet was drilled in the southeastern end of a horst to intersect the so-called Rittershoffen normal fault at the top of the basement. Based on a seismic reflection interpretation of the sedimentary cover, this fault strikes N-S, dips 45° westward and displays an apparent vertical

offset of approximately 200 m (Baujard et al., 2017). The wells penetrate the Cenozoic, Mesozoic and Permian sediments overlying the Paleozoic basement. They target the geothermal resource trapped in the fracture network at the sediment-basement interface. The bottom of the sedimentary cover is composed of sandstones deposited during the early Triassic and Permian (Aichholzer et al., 2015). The Paleozoic granitic basement, encountered at a depth of approximately 2200 m, is divided into three units: paleo weathered oxidized granite, hydrothermally altered granite and fine-grained low altered granite (Figure 2). Core studies from the exploration well at Soultz-sous-Forêts geothermal project showed that the granitic basement presents two stages of hydrothermal alteration : 1) a pervasive one which is widespread in the massif with transformation of primary minerals has given way to secondary propylitic assemblages, where chlorite is the most common phase related to the alteration of the primary biotite and 2) a vein alteration related to hydrothermal circulation developed within the fracture system which is the cause of precipitation of white mica or regular illite-smectite mixed layers associated with carbonates, iron oxides, and locally secondary quartz (Genter, 1989; Traineau et al., 1992). The upper part of the batholith shows a pronounced reddish color due to hematization related to weathering alteration and sub-horizontal joints which took place after post-orogenic exhumation.

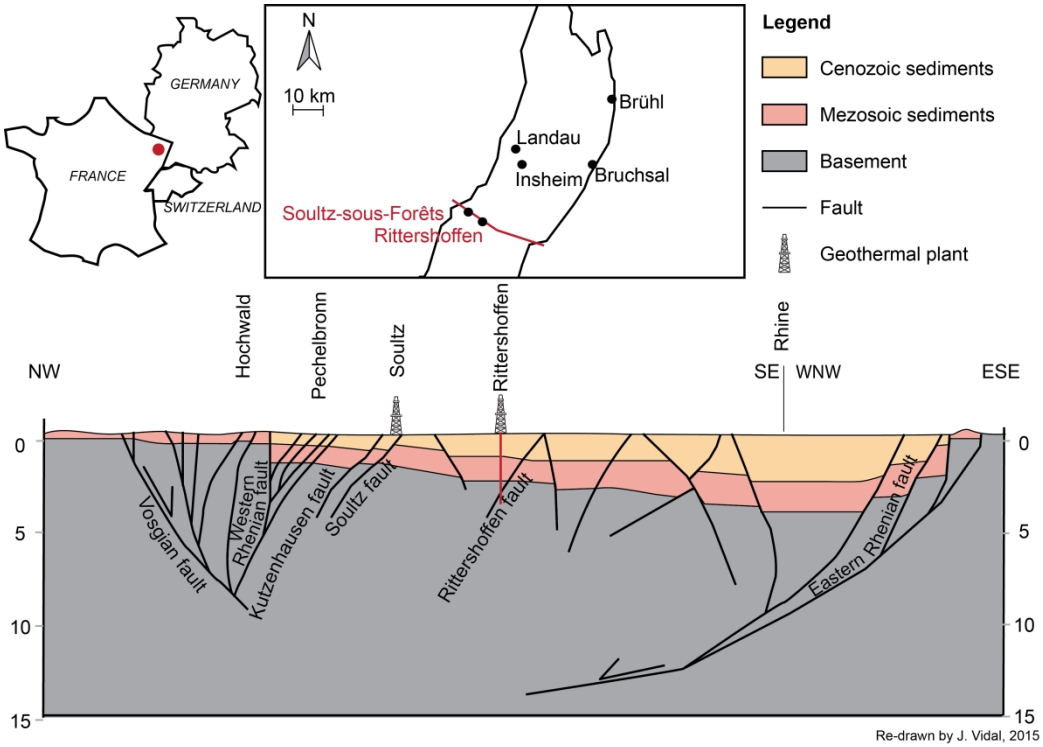

Figure 1: Location of the Rittershoffen geothermal site and geological cross section through the Upper Rhine Graben at the latitude of Rittershoffen. The interpretative trajectory of GRT-1 is represented in red on the cross section. The cross section was modified after Kappelmeyer et al. (1992) and the interpretation below 4 km depth is done by analogy to the cross section of Brun et al. (1992) and is highly speculative.

The first well, GRT-1, is nearly vertical and intersect one major permeable fracture zone between 2323 and 2368 m Measured Depth (MD) associated to a large negative temperature anomaly (Vidal et al., 2016b) (Figure 2). The natural permeability was too low for industrial exploitation and the well was successively thermally, chemically and hydraulically (TCH) stimulated (Baujard et al., 2017). The second well, GRT-2, is highly deviated to the north, an intersect one permeable fracture zone between 2535 and 2545 m MD associated to a positive temperature anomaly, one major permeable fracture between 2766 and 2800 m MD associated to a positive and a negative temperature anomaly, and two deep altered permeable zone around 2950 and 3050 m MD associated to negative temperature anomaly (Baujard et al., 2017; Vidal et al., 2016a) (Figure 2). The natural permeability expressed in term of productivity index was high enough for industrial exploitation. Geothermal water circulating into permeable fractures is higher than 160°C. Deep fluids are NaCl type with a salinity of 101 g/L and a measured pH around 6.3 (Sanjuan et al., 2016). They probably result from a mixing of primary marine brine and water of meteoric origin.

Microscopic observations of cuttings in the granitic basement of GRT-1 indicate that the top of the granitic basement down to 2380 m MD is highly hydrothermally altered with a high fracture density (Dezayes et al., 2013) (Figure 2). Two hydrothermal alteration stages were observed:1) a cataclastic stage with microquartz and illite in all the granitic samples and 2) a stage of calcite and anhydrite veins in samples above 2380 m MD. In the top of the granite ferromagnesian minerals are totally altered. Only illite is observed on bulk sample XRD analysis. Traces of pyrite are sometimes associated to illite. Dezayes et al. (2013) interprets this zone as a place of intense paleo-circulations, presently restricted between 2320 and 2380 m MD.

For this study, 21 cuttings samples were collected in the granitic basement of GRT-1 and 27 in the granitic basement of GRT-2. They were mainly collected around permeable and altered fracture zones observed in acoustic image logs and temperature logs but some samples are located in poorly zones in order to be used as reference of the pervasive alteration background.

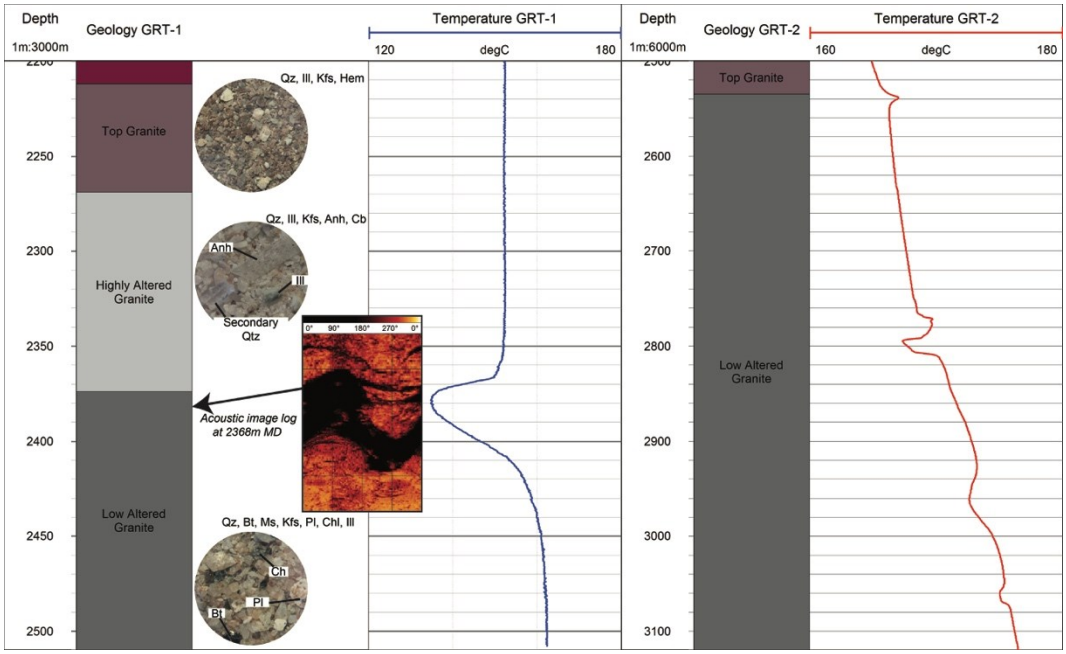

Figure 2: Temperature log in GRT-1 (in blue) and GRT-2 (in red) wells. Associated cuttings in the granitic basement of GRT-1 and acoustic image log of the main permeable fracture at 2368 m MD.

3. METHODOLOGY

XRD was performed on oriented powders of untreated and ethylene–glycol saturated samples of the fine-grained fraction (<5 µm). XRD was carried out on a Bruker D8 Advance diffractometer (CuKα radiation, 40 kV, 40 mA). Analytical conditions used for the acquisition of XRD data were as follows: angular domain: 2θ = between 2.5 and 30; step increment: 2θ = 0.025; counting time per step: 3s. XRD data acquisition and treatment were realized with the X'Pert HighScore software (PANalytical B.V.). Clay minerals were identified according to Brindley and Brown (1980).

The (001) reflection of the illitic material was deconvoluted in poorly crystallized illite (PCI), well crystallized illite (WCI) and ordered illite rich illite/smectite (I/S) mixed layer if there is any, using the Fityk software (Figure 3). Illite coherent scattering domain (CSD) size was estimated from the full width at half maximum (FWHM) intensity of the typical (001) reflection of WCI and PCI at 10 Å on the < 5 µm-fraction untreated oriented preparations (Kubler, 1968). Chlorite CSD was estimated from the FWHM intensity of the (002) reflection at 7 Å.

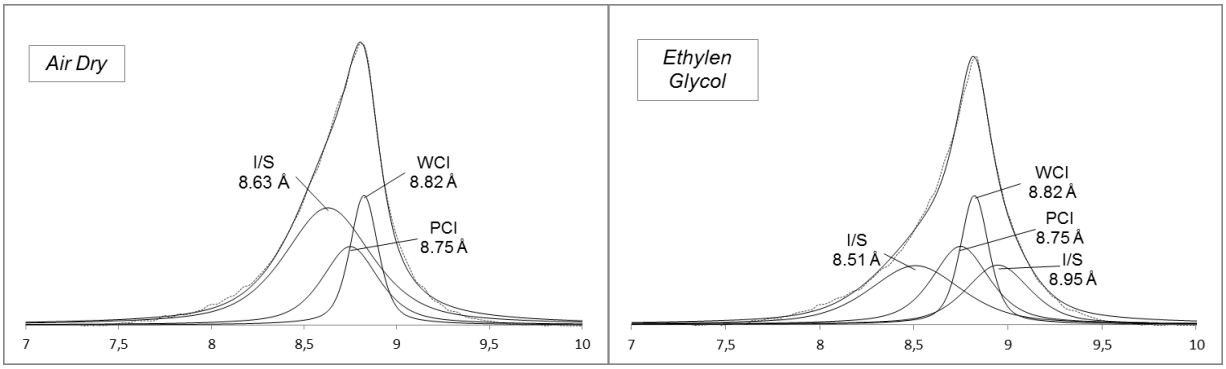

Figure 3: Deconvolution in the 7-10°2Θ CuKa domain of the X-Ray diffractograms of air dried and EG-saturated oriented powder, sample GRT-1 2218 (<5 µm clay fraction). I/S: ordered illite/smectite mixed-layer; WCI: well-crystallized illite, PCI: poorly cristallized illite

Thin sections were made from the cutting samples in order to analyze chemical composition of illite and chlorite with SEM JEOL 5600 LV equipped with a BRUKER XFlash 4030 SSD (associated with SPIRIT software). Analytical conditions were 15 kV, 1 nA, counting time 60 s, working distance 16.5 mm. Elements analyzed were Si, Al, Fe, Mg, Mn, Ti, Ca, Na and K. The system was calibrated with a variety of synthetic oxide and natural silicate standards. The reproducibility of standard analyses was close to 1% except for Na, which was 1.5%.

4. RESULTS

4.1 Mineralogy of the altered fracture zones associated to hydrothermal circulations

In GRT-1, the deepest cutting sample at 2503 m MD, corresponds to the less altered sample and is representative to the pervasive alteration background. On thin section, plagioclase phenocrysts are partially altered and partially replaced by carbonates, or illitic clay phases (Figure 4a). Biotite minerals are replaced by large-size chloritic minerals. On thin section of cuttings at 2368 m MD, a massive illitization of primary minerals associated to an intense hydrothermal alteration is observed (Figure 4b). All primary minerals are destroyed and mainly replaced by small-size illitic minerals. More rarely small-size chlorite minerals are observed. Clay materials are often associated to hematite and oxides.

In GRT-2, thin section at 2774 m MD presents an alteration stage similar to the thin section at 2503 m MD in GRT-1. Plagioclase phenocrysts are partially altered into illite and a lot of secondary quartz is observed. An illitization of minerals occurs but relicts of primary minerals are still perceptible and the structure of the rock is preserved (Figure 4c). Quartz and microquartz minerals associated to a cataclastic stage are locally observed sometimes crosscut by small cracks filled by illitic materials. Large-size (>20µm) and small-size (<5 µm) illitic minerals are identified as well as large-size (>20µm) and small-size (<5 µm) chloritic minerals (Figure 4d & e).

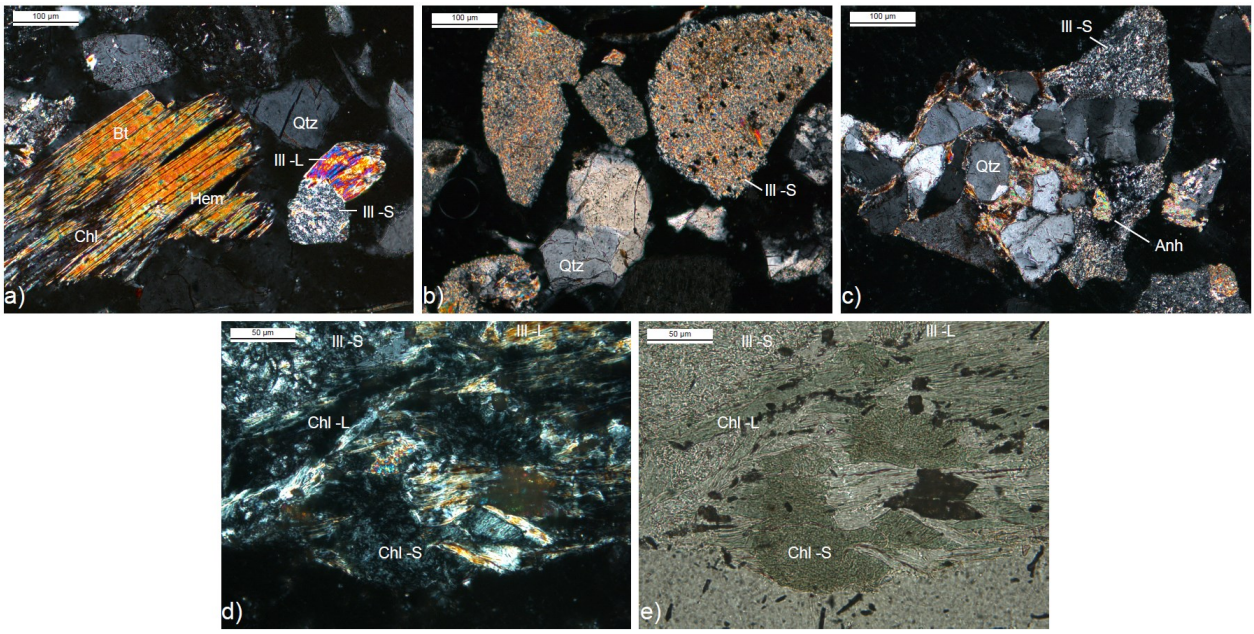

Figure 4: Microscopic observations of a) pervasive alteration at 2503 m MD in GRT-1 (LPA), b) intense secondary illitization at 2368 m MD in GRT-1 (LPA), c) illitization at 2774 m MD in GRT-2 (LPA), d) illitic and chloritic materials at 2774 m MD in GRT-2. Ill -S = small-size illitic materials, Ill -L = large-size illitic materials, Chl -S = small-size chloritic materials, Chl -L = large-size chloritic materials, Hem = hematite, Bt = Biotite, Qtz = quartz, Anh = Anhydrite

4.2 Microstructural properties of clay minerals

XRD results in GRT-1 well

In GRT-1, the presence of the PCI and the WCI is observed in all diffraction patterns. On the basis of microstructural properties of the illitic materials, three zones can be evidenced in the granite (Figure 5). At the top of the granitic basement and down to the top of the major permeable fracture zone, between 2212 and 2326 m MD, the average proportion of WCI (WCI int/(PCI int + WCI int + I/S int) is around 0.45. In this zone, the FWHM is quite constant with an average value of 0.12 °2Θ, the lowest sample at 2260 m MD (0.10 °2Θ) and the highest one at 2323 m MD (0.13 °2Θ). I/S mixed layers (less than 10% of smectite) are systematically evidenced. In the deeper samples of the drill hole below the fracture zone (from 2383 m), the proportion of WCI reaches 0.74 and 0.84 and I/S mixed layers are no more observed. WCI present slightly higher FWHM (0.17 °2Θ) than in the previous zone. The deepest sample at 2503 m MD presents highest proportion of WCI in GRT-1 (0.91) and the lowest FWMH (0.08 °2Θ). Between these two zones, in the major permeable fracture zone, from 2329 to 2377 m MD, WCI are observed in intermediate properties in terms of relative proportion, average of 0.62, and FWHM, average of 17 °2Θ. The highest FWHM in GRT-1 is 0.24 °2Θ at 2338 m MD. I/S mixed layers are not observed in the major permeable fracture zone. PCI abundance is quite constant in depth with an average proportion of 0.29. Their FWMH range from 0.25 to 0.48 °2Θ (average: 0.38 °2Θ) with the maximum value 0.48 °2Θ observed at 2354m MD.

Chloritic materials are observed in all samples at the top of the granitic from 2212 to 2329 m MD except at 2260 m MD with an average proportion of chloritic materials (Chl int/(WCI int+PCI int+I/Sint)) of 0.05 (Figure 5). Chlorite is not observed in samples (fraction > 5 µm) from the major permeable fracture zone between 2338 and 2368 m MD except the sample at 2354 m MD where the highest proportion of chloritic materials is observed in GRT-1 (0.97). Chloritic materials are observed in samples from 2377 and 2503 m MD below the major permeable fracture zone with an average proportion of chloritic materials of 0.24. The FWMH is quite constant in depth with an average value of 0.10 °2Θ, the lowest sample at 2284 m MD (0.08 °2Θ) and the highest one at 2323 m MD (0.125 °2Θ).

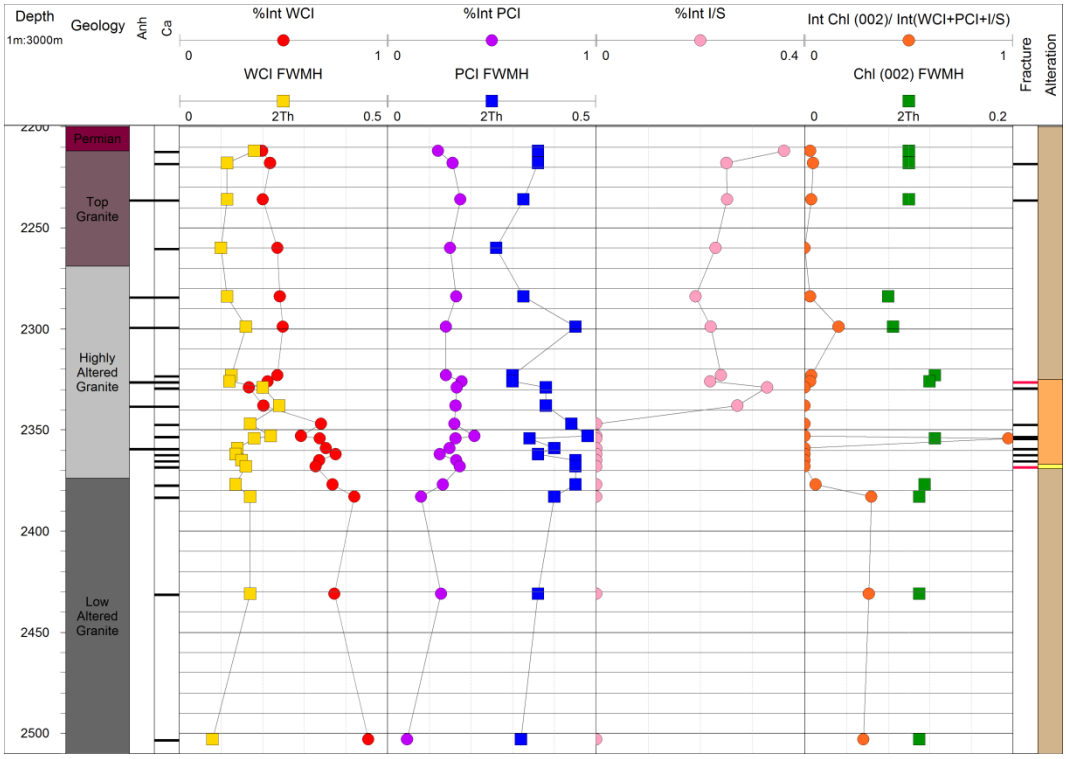

Figure 5: Microstructural properties of illitic materials and chlorite measured on XRD of the <5µm clay fraction versus depth along GRT-1 well. Red disk: WCI relative intensity; Yellow square: FWHM of WCI; Purple disk: PCI relative intensity; Blue square: FWHM of PCI; Pink disk: I/S mixed layers relative intensity; Orange disk: ratio of intensity of the (002) reflection of chlorite over the intensity of the (001) reflection of the illitic materials; Green square: FWHM of the (002) reflection of chlorite. Presence of Anhydrite (Anh) and Calcite (Ca) on XRD is indicated by a black line at the sample depth. Occurrence of fracture (black) and permeable fracture (red) is derivd from acoustic image log observations (Vidal et al., 2016b). Alteration grades are evaluated from geophysical logs analysis (Vidal et al., 2016b). Yellow: quartz- and clay-rich cataclastic zone associated to fault core; Light orange: altered and porous damage zone; Light brown: altered granite.

XRD results in GRT-2 well

In GRT-2, the presence of the PCI and the WCI is observed in all diffraction patterns (Figure 6). The proportion of WCI in samples of the poorly granite is between 0.73 and 1 with an average value of 0.85. The proportion of WCI decreases in samples at 2533 (0.56), 2773 (0.65), 2785 (0.61) and 3052 m MD (0.56). In these samples, I/S mixed layers (less than 10% of smectite) are also observed. WCI present similar FWHM in all samples with an average value of 0.13 °2Θ with the lowest value (0.095 °2Θ) at 3064 m MD and the highest one (0.18 °2Θ) at 3052 m MD. PCI properties seem to be quite similar in all samples. The average proportion of PCI is 0.16 with the highest sample (0.28) at 3052 m MD and the average FWMH of 0.30 °2Θ with the lowest sample (0.18 °2Θ) at 3052 m MD and the highest one (0.40 °2Θ) at 3058 m MD.

Chloritic materials are observed in all samples in the granitic basement of GRT-2 (Figure 6). The average proportion of chloritic materials is 0.38 in the granitic basement with the lowest sample (0.02) at 2652 m MD and the highest one (1.35) at 3190 m MD. The FWMH is quite constant with the average value of 0.12 °2Θ, the lowest sample at 2652 m MD (0.09 °2Θ) and the highest one at 2533 m MD (0.18 °2Θ).

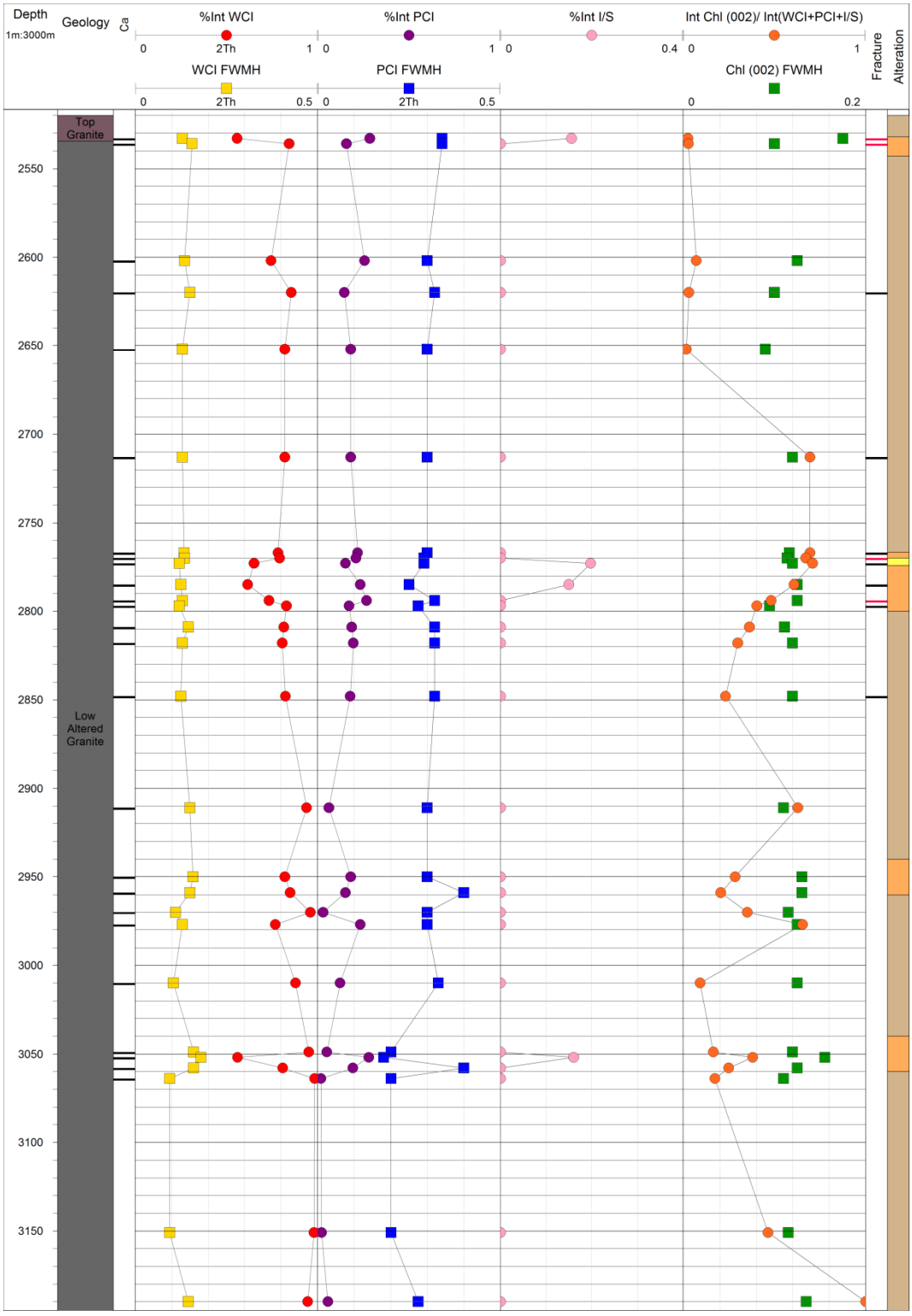

Figure 6: Microstructural properties of illitic materials and chlorite measured on XRD of the <5µm clay fraction versus depth along GRT-2 well. Red disk: WCI relative intensity; Yellow square: FWHM of WCI; Purple disk: PCI relative intensity; Blue square: FWHM of PCI; Pink disk: I/S mixed layers relative intensity; Orange disk: ratio of intensity of the (002) reflection of chlorite over the intensity of the (001) reflection of the illitic materials; Green square: FWHM of the (002) reflection of chlorite. Presence of Calcite (Ca) on XRD is indicated by a black line at the sample depth. Occurrence of fracture (black) and permeable fracture (red) is derived from acoustic image log observations (Vidal et al., 2016a). Alteration grades are evaluated from geophysical logs analysis (Vidal et al., 2016a). Yellow: quartz- and clay-rich cataclastic zone associated to fault core; Light orange: altered and porous damage zone; Light brown: altered granite.

4.3 Chemical compositions of clay minerals

SEM results in GRT-1 well

The structural formulae of illitic materials are calculated on the basis of 11 oxygens, assuming the total irons as Fe^{3+} (Table 1). Chemical analyses of illitic material (WCI+PCI +I/S ml) do not present major variations. The interlayer charge is between 0.83 and 0.90 and the average octahedral Al content is 1.67+/-0.05 per $O_{10}(OH)$. The average Fe and Mg contents are 0.14+/-0.05 and 0.18+/-0.07 at the top of the granitic basement. The ratio Fe/Mg is <1 for samples at 2212, 2218, 2236, 2284, 2326, 2329 m MD. The average Fe and Mg contents are 0.14+/-0.05 and 0.13+/-0.04 in the major permeable fracture zone and in the deep granitic basement. The ratio Fe/Mg is ≥1 for samples at 2338, 2365, 2368, 2377 and 2503 m MD. Nevertheless, the standard deviation of chemical analyses decreases with depth underlying more homogeneous illitic materials in the deeper part outside the permeable fracture zone.

The structural formulae of chloritic materials are calculated on the basis of 14 oxygens, assuming the total irons as Fe^{2+} (Table 2). The octahedral occupancy is between 5.80 and 5.94 and the octahedral Al is higher than tetrahedral Al. An iron-rich chlorite is observed in samples at 2212m MD (XFe=0.80) and 2368 m MD (XFe=0.83) at the top of the granitic and in the major permeable fracture zone (Figure 7). A ferromagnesian chlorite which is relatively depleted in iron compared to the chlorite at the top of the granitic basement is again observed in the deepest granitic samples at 2503 m MD (XFe=0.38).

Table 1 Chemical analyses of some illitic materials at various depths in GRT-1 and GRT-2 wells. n.a.: number of analyses; An. Av.: analytical average; s.d.: standard deviation; OCT: octahedral occupancy; INTCH: interlayer charge.

Samples	GRT-1 2212		GRT-1 2218		GRT-1 2236		GRT-1 2284		GRT-1 2326		GRT-1 2329		GRT-1 2338		GRT-1 2365		GRT-1 2368		GRT-1 2377		GRT-1 2503	
n. a.	13		18		15		14		29		22		21		46		52		19		22	
	An. Av.	s.d.	An. Av.	s.d.	An. Av.	s.d.	An. Av.	s.d.	An. Av.	s.d.	An. Av.	s.d.	An. Av.	s.d.	An. Av.	s.d.	An. Av.	s.d.	An. Av.	s.d.	An. Av.	s.d.
Si	3,35	*0,25*	3,28	*0,20*	3,36	*0,02*	3,40	*0,04*	3,31	*0,19*	3,38	*0,12*	3,44	*0,29*	3,30	*0,06*	3,34	*0,12*	3,31	*0,08*	3,33	*0,06*
Al IV	0,65	*0,25*	0,72	*0,20*	0,64	*0,02*	0,60	*0,04*	0,69	*0,19*	0,62	*0,12*	0,56	*0,29*	0,70	*0,06*	0,66	*0,12*	0,69	*0,08*	0,67	*0,06*
Al VI	1,66	*0,18*	1,73	*0,11*	1,61	*0,13*	1,63	*0,06*	1,71	*0,21*	1,66	*0,07*	1,67	*0,07*	1,68	*0,04*	1,65	*0,09*	1,72	*0,07*	1,74	*0,06*
Fe 3+	0,13	*0,08*	0,11	*0,03*	0,18	*0,09*	0,16	*0,04*	0,13	*0,07*	0,14	*0,00*	0,14	*0,06*	0,16	*0,04*	0,17	*0,05*	0,14	*0,03*	0,11	*0,04*
Mg	0,21	*0,10*	0,16	*0,06*	0,19	*0,02*	0,19	*0,04*	0,15	*0,14*	0,18	*0,06*	0,14	*0,04*	0,14	*0,01*	0,16	*0,05*	0,12	*0,04*	0,11	*0,05*
Ti	0,01	*0,01*	0,01	*0,01*	0,00	*0,00*	0,00	*0,00*	0,00	*0,00*	0,00	*0,00*	0,00	*0,00*	0,00	*0,00*	0,00	*0,00*	0,00	*0,00*	0,00	*0,00*
Mn	0,00	*0,00*	0,00	*0,00*	0,00	*0,00*	0,00	*0,00*	0,00	*0,00*	0,00	*0,00*	0,00	*0,00*	0,00	*0,00*	0,00	*0,00*	0,00	*0,00*	0,00	*0,00*
OCT	2,00	*0,02*	2,01	*0,03*	1,99	*0,01*	1,98	*0,02*	1,99	*0,00*	1,99	*0,02*	1,95	*0,11*	1,98	*0,02*	1,98	*0,05*	1,99	*0,01*	1,96	*0,02*
Ca	0,01	*0,00*	0,01	*0,02*	0,00	*0,00*	0,00	*0,00*	0,00	*0,00*	0,00	*0,00*	0,00	*0,00*	0,00	*0,00*	0,01	*0,03*	0,00	*0,00*	0,04	*0,04*
Na	0,00	*0,01*	0,00	*0,01*	0,00	*0,00*	0,00	*0,00*	0,00	*0,00*	0,00	*0,00*	0,00	*0,00*	0,00	*0,02*	0,00	*0,00*	0,00	*0,00*	0,00	*0,00*
K	0,83	*0,08*	0,84	*0,04*	0,86	*0,04*	0,85	*0,03*	0,86	*0,06*	0,82	*0,01*	0,84	*0,14*	0,89	*0,05*	0,86	*0,05*	0,85	*0,05*	0,86	*0,04*
INTCH	0,85	*0,08*	0,85	*0,05*	0,87	*0,04*	0,85	*0,03*	0,86	*0,06*	0,83	*0,01*	0,84	*0,14*	0,90	*0,02*	0,87	*0,05*	0,85	*0,04*	0,90	*0,07*

Samples	GRT-2 2770		GRT-2 2773		GRT-2 2794		GRT-2 2950		GRT-2 2977		GRT-2 3052	
n. a.	21		15		18		29		24		20	
	An. Av.	s.d.	An. Av.	s.d.	An. Av.	s.d.	An. Av.	s.d.	An. Av.	s.d.	An. Av.	s.d.
Si	3,32	*0,15*	3,31	*0,09*	3,35	*0,03*	3,32	*0,01*	3,33	*0,02*	3,35	*0,00*
Al IV	0,68	*0,15*	0,69	*0,09*	0,65	*0,03*	0,68	*0,01*	0,67	*0,02*	0,65	*0,00*
Al VI	1,62	*0,20*	1,64	*0,05*	1,59	*0,07*	1,68	*0,03*	1,68	*0,04*	1,60	*0,02*
Fe 3+	0,17	*0,08*	0,17	*0,01*	0,19	*0,02*	0,15	*0,03*	0,15	*0,05*	0,19	*0,02*
Mg	0,18	*0,11*	0,18	*0,04*	0,20	*0,06*	0,15	*0,01*	0,15	*0,01*	0,19	*0,04*
Ti	0,00	*0,01*	0,01	*0,00*	0,00	*0,00*	0,00	*0,00*	0,00	*0,00*	0,00	*0,00*
Mn	0,00	*0,00*	0,00	*0,00*	0,00	*0,00*	0,00	*0,00*	0,00	*0,00*	0,00	*0,00*
OCT	1,99	*0,01*	1,99	*0,00*	1,98	*0,01*	1,99	*0,01*	1,99	*0,00*	1,98	*0,00*
Ca	0,00	*0,00*	0,00	*0,00*	0,00	*0,00*	0,00	*0,00*	0,00	*0,00*	0,01	*0,00*
Na	0,00	*0,00*	0,00	*0,00*	0,00	*0,00*	0,00	*0,00*	0,00	*0,00*	0,00	*0,00*
K	0,90	*0,02*	0,89	*0,04*	0,89	*0,01*	0,86	*0,00*	0,84	*0,02*	0,87	*0,03*
INTCH	0,91	*0,02*	0,89	*0,04*	0,90	*0,01*	0,87	*0,00*	0,85	*0,01*	0,88	*0,04*

Table 2 Chemical analyses of some chloritic materials at various depths of GRT-1 and GRT-2 wells. n.a.: number of analyses; An Av: analytical average; s.d.: standard deviation; OCT: octahedral occupancy; INTCH: interlayer charge; an. loc.: microsite of crystallization; Fe–Mg: chlorite in replacement of primary ferromagnesian minerals; Vug: chlorite crystallized in vugs.

Samples	GRT-1 2212		GRT-1 2368		GRT-1 2503		GRT-2 2770		GRT-2 2773		GRT-2 2773		GRT2 2794	GRT-2 2950		GRT-2 2950		GRT-2 2977		GRT-2 3052	
an. loc.	Vug		Vug		FeMg		FeMg		FeMg		Vug		Vug	FeMg		Vug		FeMg		FeMg	
n. a.	7		10		6		2		3		4		1	2		2		5		7	
	An. Av.	s.d.	An. Av.	s.d.	An. Av.	s.d.	An. Av.	s.d.	An. Av.	s.d.	An. Av.	s.d.		An. Av.	s.d.	An. Av.	s.d.	An. Av.	s.d.	An. Av.	s.d.
Si	2,81	*0,03*	2,81	*0,04*	3,07	*0,10*	2,88	*0,01*	2,88	*0,05*	2,84	*0,07*	2,81	2,97	*0,05*	2,90	*0,04*	3,00	*0,09*	2,90	*0,01*
Al IV	1,19	*0,03*	1,19	*0,04*	0,93	*0,10*	1,12	*0,01*	1,12	*0,05*	1,16	*0,07*	1,19	1,03	*0,05*	1,10	*0,04*	1,00	*0,09*	1,10	*0,01*
Al VI	1,24	*0,04*	1,28	*0,04*	1,22	*0,06*	1,22	*0,01*	1,76	*0,10*	1,68	*0,13*	1,37	1,15	*0,07*	1,30	*0,07*	1,21	*0,02*	1,20	*0,05*
Ti	0,00	*0,00*	0,01	*0,01*	0,03	*0,05*	0,01	*0,00*	0,00	*0,00*	0,00	*0,01*	0,01	0,01	*0,00*	0,01	*0,00*	0,01	*0,01*	0,01	*0,00*
Fe 2+	3,77	*0,24*	3,81	*0,25*	1,70	*0,16*	2,01	*0,12*	2,18	*0,12*	3,67	*0,32*	3,13	1,97	*0,16*	2,92	*0,08*	1,92	*0,07*	2,01	*0,11*
Mn 2+	0,01	*0,00*	0,01	*0,00*	0,07	*0,04*	0,04	*0,04*	0,04	*0,02*	0,01	*0,01*	0,01	0,05	*0,03*	0,01	*0,00*	0,07	*0,00*	0,05	*0,04*
Mg 2+	0,92	*0,20*	0,79	*0,23*	2,78	*0,09*	2,65	*0,05*	2,39	*0,15*	0,91	*0,18*	1,35	2,74	*0,22*	1,62	*0,05*	2,65	*0,02*	2,67	*0,01*
OCT	5,94	*0,04*	5,90	*0,05*	5,80	*0,08*	5,93	*0,01*	5,90	*0,03*	5,90	*0,03*	5,87	5,92	*0,02*	5,86	*0,07*	5,87	*0,07*	5,93	*0,03*
Ca	0,02	*0,02*	0,04	*0,07*	0,01	*0,01*	0,00	*0,01*	0,00	*0,00*	0,01	*0,02*	0,03	0,01	*0,00*	0,02	*0,01*	0,01	*0,00*	0,01	*0,01*
Na	0,00	*0,00*	0,00	*0,00*	0,00	*0,00*	0,00	*0,00*	0,00	*0,00*	0,00	*0,00*	0,00	0,00	*0,00*	0,00	*0,00*	0,00	*0,00*	0,00	*0,00*
K	0,01	*0,01*	0,02	*0,01*	0,04	*0,04*	0,01	*0,00*	0,00	*0,00*	0,01	*0,01*	0,00	0,00	*0,00*	0,02	*0,02*	0,03	*0,04*	0,01	*0,00*
INTCH	0,05	*0,04*	0,11	*0,14*	0,05	*0,04*	0,01	*0,01*	0,01	*0,00*	0,04	*0,02*	0,06	0,02	*0,00*	0,06	*0,04*	0,04	*0,05*	0,02	*0,01*
Fe/(Fe+Mg)	0,80	*0,04*	0,83	*0,05*	0,38	*0,03*	0,43	*0,02*	0,48	*0,03*	0,80	*0,05*	0,70	0,42	*0,04*	0,64	*0,00*	0,42	*0,01*	0,43	*0,01*

SEM results in GRT-2 well

In GRT-2 well, as in GRT-1, chemical analyses of illitic material (WCI+PCI +I/S ml) do not present major variations (Table 1). The interlayer charge is between 0.85 and 0.91 and the average octahedral Al content is 1.63+/-0.07 per $O_{10}(OH)$. The average Fe and Mg contents are 0.17+/-0.03 and 0.18+/-0.05 in the granitic basement. The ratio Fe/Mg is ≥1 for samples at 2338, 2365, 2368, 2377 and

2503 m MD. Nevertheless, the standard deviation of chemical analyses decreases with depth underlying more homogeneous illitic materials in the deeper part outside the permeable fracture zone.

In the chloritic materials, octahedral Al is higher than tetrahedral Al (Table 2). The octahedral occupancy is between 5.86 and 5.93. An iron-rich chlorite (XFe>0.60) is observed in samples at 2773, 2794, 2950 in the major permeable fracture zone and in one altered permeable zone in the deepest granitic basement. A ferromagnesian chlorite (XFe=0.33-0.48) which is relatively depleted in iron is observed in samples 2770, 2773, 2950, 2977 and 3052 m MD int the major permeable fracture zone and in the deeper altered and unaltered granitic basement (Figure 7).

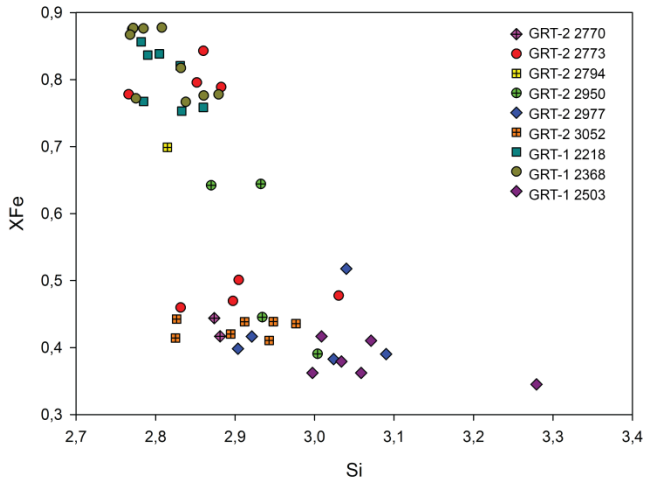

Figure 7: Plot of some chlorite analyses in Fe/(Fe+Mg) (XFe) versus Si diagram for GRT-1 and GRT-2 wells.

5. DISCUSSION

5.1 Signature of illitic materials

The illitic material properties evidenced that GRT1 and GRT2 do not display the same hydrothermal alteration profile. A highly altered zone at the top granite is evidenced only for GRT1. This clay rich zone is expressed by illite rich illite/smectite mixed layers + illite of small size crystallites (increased abundance of PCI and FWHM). Outside permeable fracture zones, illitic material displays quite constant crystal structures properties (proportions of WCI, PCI, FWHM, absence of I/S) and stable chemical properties both in GRT1 and GRT2. Regarding the clay signature of permeable levels, in GRT-1, in the major permeable fracture zone, from 2320 to 2380 m MD, the proportion of the WCI is lower than the bottom low altered granite, I/S mixed layers are observed at the top of the zone and the PCI crystallinity is lower at the bottom of the zone (Figure 5). In GRT-2, in the permeable fracture zones at 2533 m MD and from 2765 to 2800 m MD, the proportion of WCI decreases and I/S mixed layers are observed (Figure 6). Around 2960 m MD, the PCI crystallinity is lower. Between 3050 and 3060 m MD, the proportion of WCI decreases, I/S mixed layers are observed and the PCI crystallinity is lower. In both wells, the crystallinity (along the c axis) of the illitic materials decreases in permeable zones as reflected by the higher FWMH of PCI and the presence of I/S mixed layers. In both wells, the granitic primary rock composition is approximately homogeneous as well as the nature of geothermal fluids collected (Sanjuan et al., 2016). The microstructural properties of the illitic materials are known to be potential indicators of fluid circulations and paleo-circulations (Flexser, 1991; Harvey and Browne, 1991; Mas et al., 2003, 2006; Patrier et al., 1996; Teklemariam et al., 1996). In permeable fracture zone which channels the ascending geothermal fluids strongly oversaturated with respect to clay minerals, abrupt changes flow regime such as mixing of geothermal fluids lead to explosive nucleation of clay crystallites with low size and promote the occurrence of heterogeneous mineral assemblages such as I/S mixed layers (Beaufort et al., 1996; Patrier et al., 1996). As seen from cutting microscopic observations in GRT-1 and GRT-2, in permeable fracture zones, small-size illitic materials predominate.

The chemical compositions of illitic materials are quite homogeneous in all samples except at the top of the granitic basement in GRT-1 where Mg content is higher (Table 1). This could be explained by some basin fluids exchanges from the sedimentary cover and chemical measurements of illite in overlying sandstones will be carried out to investigate this hypothesis.

5.2 Signature of chloritic materials

Two populations of chloritic materials were observed in GRT-1 and GRT-2 (Table 2, Figure 7). Ferromagnesian chloritic materials, associated to pervasive alteration, occur in all the granitic batholite. They result from biotite alteration under oxidizing conditions. It has been demonstrated that during pervasive alteration, the chemistry of the chloritic materials is rock dominated (Beaufort et al., 1992; López-Munguira et al., 2002; Mas et al., 2006). The magnesium incorporation is promoted in the structure of chlorite which crystallize with iron oxides such as hematite or magnetite under oxidizing conditions (Beaufort et al., 1992). Iron-rich chloritic materials, associated to hydrothermal alteration, occur in permeable fracture zones. It has been demonstrated that the chemistry of iron-rich chloritic materials is probably controlled by the fluid circulating into permeable fracture zone in reducing conditions (Beaufort et al., 1992; Mas et al., 2006; Patrier et al., 1996).

Both chloritic populations do not crystallize during the same mineralogical events and the pervasive alteration probably took place at higher temperature. In GRT-1, the rare presence of chloritic materials could be explained by a quasi-total dissolution of chlorites during paleo-circulations and the massive illitization of the permeable fracture zone (Figure 5). Due to high water/rock ratio related to massive fluid circulation in the natural fracture system, intense vein alteration took place and transformed successively primary biotite into chlorite and then into illite.

6. CONCLUSION

The study of clay minerals in geothermal wells GRT-1 and GRT-2 at Rittershoffen confirms the presence of permeable fracture zones that channel geothermal fluids. Illitic phases which precipitate during fluid circulation have specific microstructural properties in particular, the decrease of their crystallinity and the specific apparition of I/S mixed layers. In response to mixing of oversaturated fluids with contrasting temperatures, the nucleation rate predominates over growth rate favoring small-size clay crystallites and metastable phases. In GRT-1, the intensive illitization of the top of the granitic basement and the major permeable fracture zone reflects paleo-circulations that probably plug the fracture system and contribute to the actual low natural pre-stimulation permeability. In GRT-2, hydrothermal alteration and illitization are less pronounced than in GRT-1 that could partly explain the higher natural permeability of the fracture system. The ferromagnesian chloritic materials, the iron-rich chloritic materials and the illitic materials belong to different clay paragenesis. These first conclusions are promising and underline the importance of studying clay minerals for permeable fracture zone prospection into the Rittershoffen geothermal reservoir.

ACKNOWLEDGMENTS

This work was based on data from the geothermal project at Rittershoffen, France. The authors acknowledge the ECOGI project, owner of the geological and geophysical log data as well as the cutting samples. A part of the logs were collected thanks to the EGS Alsace project, co-founded by ADEME (French Agency for Environment and Energy). The participation to the 42nd Workshop on Geothermal Reservoir Engineering at Stanford University was prepared as a contribution to the PhD thesis of Jeanne Vidal, co-funded by ADEME and the LabEx G-Eau-Thermie Profonde, which is co-funded by the French government under the program “Investissements d’Avenir”.

REFERENCES

Aichholzer, C., Duringer, P., Orciani, S., Genter, A., 2015. New stratigraphic interpretation of the twenty-eight-year old GPK-1 geothermal well of Soultz-sous-Forêts (Upper Rhine Graben, France), in: Proceedings of the 4th European Geothermal Workshop. Strasbourg, France.

Baujard, C., Genter, A., Dalmais, E., Maurer, V., Hehn, R., Rosillette, R., Vidal, J., Schmittbuhl, J., 2017. Hydrothermal characterization of wells GRT-1 and GRT-2 in Rittershoffen, France: Implications on the understanding of natural flow systems in the rhine graben. Geothermics 65, 255–268. doi:10.1016/j.geothermics.2016.11.001

Beaufort, D., Papapanagiotou, P., Patrier Mas, P., Fouillac, A.M., Traineau, H., 1996. I/S and C/S Mixed Layers, Some Indicators of Recent Physical-Chemical Changes in Active Geothermal Systems: The Case Study of Chipilapa (El Salvador), in: Proceedings of Seventeenth Workshop on Geothermal Reservoir Engineering. Stanford University, California, USA.

Beaufort, D., Patrier, P., Meunier, A., Ottaviani, M.M., 1992. Chemical variations in assemblages including epidote and/or chlorite in the fossil hydrothermal system of Saint Martin (Lesser Antilles). Journal of Volcanology and Geothermal Research 51, 95–114. doi:10.1016/0377-0273(92)90062-I

Brindley, G.W., Brown, G., 1980. Crystal structures of clay minerals and their X-ray identification., Mineralogy Society London. ed. Brindley G.W. and Brown G.

Brun, J.P., Gutscher, M.-A., DEKORP-ECORS teams, 1992. Deep crustal structure of the Rhine Graben from dekorp-ecors seismic reflection data: A summary. Tectonophysics 208, 139–147. doi:10.1016/0040-1951(92)90340-C

Dezayes, C., Sanjuan, B., Gal, F., Lerouge, C., Brach, M., 2013. Forage d’exploration géothermique GRT1 : suivi géochimique des fluides et caractérisation des zones fracturées (Rapport confidentiel pour ECOGI No. RP-62546-FR). BRGM.

Flexser, S., 1991. Hydrothermal alteration and past and present thermal regimes in the western moat of Long Valley caldera. Journal of Volcanology and Geothermal Research 48, 303–318. doi:10.1016/0377-0273(91)90048-5

Genter, A., 1989. Géothermie roches chaudes sèches: le granite de Soultz-sous-Forêts (Bas-Rhin, France). Fracturation naturelle, altérations hydrothermales et interaction eau-roche, Document du BRGM 185. Université d’Orléans.

Harvey, C.C., Browne, P.R.L., 1991. Mixed-layer clay geothermometry in the Wairakei geothermal field, New Zealand. Clays and Clay Minerals 39, 614–621.

Kappelmeyer, O., Gérard, A., Schloemer, R., Ferrandes, F., Rummel, F., Benderitter, Y., 1992. European HDR Project at Soultz-sous-Forêts: General Presentation, in: Geothermal Energy in Europe - The Soultz Hot Dry Rock Project. James C. Bresee, Montreux, Switzerland.

Kubler, B., 1968. Evaluation quantitative du métamorphisme par la cristallinité de l’illite: Etat des progrès réalisés ces dernières années. Bulletin du Centre de Recherches de Pau-SNPA 2, 385–397.

López-Munguira, A., Nieto, F., Morata, D., 2002. Chlorite composition and geothermometry: a comparative HRTEM/AEM-EMPA-XRD study of Cambrian basic lavas from the Ossa Morena Zone, SW Spain. Clay Minerals 37, 267–281. doi:10.1180/0009855023720033

Mas, A., Guisseau, D., Patrier Mas, P., Beaufort, D., Genter, A., Sanjuan, B., Girard, J.P., 2006. Clay minerals related to the hydrothermal activity of the Bouillante geothermal field (Guadeloupe). Journal of Volcanology and Geothermal Research 158, 380–400. doi:10.1016/j.jvolgeores.2006.07.010

Mas, A., Patrier, P., Beaufort, D., Genter, A., 2003. Clay-mineral signatures of fossil and active hydrothermal circulations in the geothermal system of the Lamentin Plain, Martinique. Journal of Volcanology and Geothermal Research 124, 195–218. doi:10.1016/S0377-0273(03)00044-1

Patrier, P., Papapanagiotou, P., Beaufort, D., Traineau, H., Bril, H., Rojas, J., 1996. Role of permeability versus temperature in the distribution of the fine (< 0.2 μm) clay fraction in the Chipilapa geothermal system (El Salvador, Central America). Journal of Volcanology and Geothermal Research 72, 101–120. doi:10.1016/0377-0273(95)00078-X

Pribnow, D., Schellschmidt, R., 2000. Thermal tracking of upper crustal fluid flow in the Rhine Graben. Geophysical Research Letters 27.

Reyes, A.G., 1990. Petrology of Philippine geothermal systems and the application of alteration mineralogy to their assessment. Journal of Volcanology and Geothermal Research 43, 279–309. doi:10.1016/0377-0273(90)90057-M

Sanjuan, B., Millot, R., Innocent, C., Dezayes, C., Scheiber, J., Brach, M., 2016. Major geochemical characteristics of geothermal brines from the Upper Rhine Graben granitic basement with constraints on temperature and circulation. Chemical Geology 428, 27–47. doi:10.1016/j.chemgeo.2016.02.021

Schellschmidt, R., Clauser, C., 1996. The thermal regime of the Upper Rhine Graben and the anomaly at Soultz. Zeitschrift für Angewandte Geologie 42, 40–44.

Teklemariam, M., Battaglia, S., Gianelli, G., Ruggieri, G., 1996. Hydrothermal alteration in the Aluto-Langano geothermal field, Ethiopia. Geothermics 25, 679–702. doi:10.1016/S0375-6505(96)00019-3

Traineau, H., Genter, A., Cautru, J.-P., Fabriol, H., Chèvremont, P., 1992. Petrography of the granite massif from drill cutting analysis and well log interpretation in the geothermal HDR borehole GPK-1 (Soultz, Alsace, France), in: Geothermal Energy in Europe - The Soultz Hot Dry Rock Project. James C. Bresee, Montreux, Switzerland, pp. 1–29.

Vidal, J., Genter, A., Chopin, F., Dalmais, E., 2016a. Natural fractures and permeability at the geothermal site Rittershoffen, France, in: Proceedings of European Geothermal Congress 2016. Strasbourg, France.

Vidal, J., Genter, A., Schmittbuhl, J., 2016b. Pre- and post-stimulation characterization of geothermal well GRT-1, Rittershoffen, France: insights from acoustic image logs of hard fractured rock. Geophys. J. Int. 206, 845–860. doi:10.1093/gji/ggw181